



HAL
open science

Design of surface ligands for blood compatible gold nanoparticles: Effect of charge and binding energy

Jordan Beurton, Philippe Lavalle, Arnaud Pallotta, Thomas Chaigneau, Igor Clarot, Ariane Boudier

► **To cite this version:**

Jordan Beurton, Philippe Lavalle, Arnaud Pallotta, Thomas Chaigneau, Igor Clarot, et al.. Design of surface ligands for blood compatible gold nanoparticles: Effect of charge and binding energy. International Journal of Pharmaceutics, 2020, 580, pp.119244. 10.1016/j.ijpharm.2020.119244 . hal-02922664

HAL Id: hal-02922664

<https://hal.univ-lorraine.fr/hal-02922664>

Submitted on 22 Aug 2022

HAL is a multi-disciplinary open access archive for the deposit and dissemination of scientific research documents, whether they are published or not. The documents may come from teaching and research institutions in France or abroad, or from public or private research centers.

L'archive ouverte pluridisciplinaire **HAL**, est destinée au dépôt et à la diffusion de documents scientifiques de niveau recherche, publiés ou non, émanant des établissements d'enseignement et de recherche français ou étrangers, des laboratoires publics ou privés.



Distributed under a Creative Commons Attribution - NonCommercial 4.0 International License

1 **Design of surface ligands for blood compatible gold nanoparticles: effect of charge and**
2 **binding energy**

3 **Jordan Beurton^{1,2}, Philippe Lavalle², Arnaud Pallotta¹, Thomas Chaigneau¹, Igor**
4 **Clarot¹, Ariane Boudier^{1*}**

5 **Adresses**

6 ¹: Université de Lorraine, CITHEFOR, Nancy, France

7 ²: Université de Strasbourg, Faculty of Medicine, Inserm UMR 1121 Biomaterials and
8 Bioengineering, Strasbourg, France

9 *Corresponding author: ariane.boudier@univ-lorraine.fr

10

11

12

13

14

15

16 **Abstract**

17 Gold nanoparticle (AuNP) interaction with the blood compartment as a function of their
18 charge and the binding energy of their surface ligand was explored. Citrate, polyallylamine
19 and cysteamine stabilized AuNP along with dihydrolipoic acid and polyethylene glycol
20 capped AuNP were synthesized and fully characterized. Their interactions with model
21 proteins (human albumin and human fibrinogen) were studied. Complexes formed between
22 AuNP and protein revealed several behaviors ranging from corona formation to aggregation.
23 Protein fluorescence quenching as a function of temperature and AuNP concentration allowed
24 the determination of the thermodynamic parameters describing these interactions. The
25 hemolysis induced by AuNP was also probed: an increasing or a decreasing of hemolysis ratio
26 induced by AuNP was observed as of function of protein corona formation. Taken together,
27 our results drew up a composite sketch of an ideal surface ligand for blood compatible AuNP.
28 This capping agent should be strongly bound to the gold core by one or more thiol groups and
29 it must confer a negative charge to the particles.

30 **Keywords:** Inorganic Nanoparticles, Surface Chemistry, Protein Adsorption, Thermodynamic
31 Parameters, Hemolysis

32

33 1. Introduction

34

35 Gold nanoparticles (AuNP) are part of the most developed and used nanomaterials because of
36 their ease of synthesis and their characteristics. They are well defined by their
37 physicochemical and optical properties. AuNP can be functionalized by biomolecules and
38 drugs with important yields due to a huge surface over volume ratio (Daniel & Astruc, 2004).

39 The abundance of possible ligands creates a wide variety of objects, in terms of surface
40 charge (zeta potential) or hydrodynamic diameter. The newly synthesized particles are
41 surrounded by a more or less displaceable shell depending on the ligand binding energy.

42 Among their various uses, these particles can be used as biosensors, drug delivery systems or
43 contrast agents (Mieszawska et al., 2013) involving their intravenous injection. The

44 bloodstream is a highly complex medium in which AuNP can interact with a wide variety of
45 proteins or cells. According to the Vroman's effect (Vroman, 1962), the interaction between

46 AuNP and plasma proteins is a dynamic system. During this sequential adsorption, a
47 heterogeneous corona is formed with proteins with an increasing affinity for the AuNP. This
48 phenomenon determines the biological identity of the particles and manages not only their
49 bioavailability and pharmacokinetics but also their possible toxicity (Wang et al., 2015).

50 Several studies already probed the interaction of proteins with AuNP as a function of their
51 size, shape, charge... As examples, the variation of the nanoparticle hydrodynamic diameter

52 revealed an influence on their internalization in cells through endocytosis or micropinocytosis
53 or in hemolysis induction (Purohit et al., 2016). Lacerda *et al.*, reported an increasing affinity

54 between fibrinogen and citrate capped AuNP as a function of their hydrodynamic diameters
55 (Lacerda et al., 2010). A shape dependence in the protein activation and cellular uptake was

56 also described. Xie *et al.*, observed an increased internalization linked to AuNP shape (from
57 stars and rods to triangles, respectively) (Xie et al., 2017). Quach and Kah demonstrated that

58 gold nano-spheres, -stars and -rods bearing polyethylene glycol (PEG) groups were able to
59 induce complement activation (Quach and Kah, 2017). Through all these studies, all types of
60 interactions between NP and proteins have been reported, from the weakest (Van der Walls
61 and/or hydrogen bonds) to the strongest (covalent bound) (Shemetov et al., 2012). Thus,
62 ligand exchange phenomena (NP surface ligand vs blood protein), especially with low-energy
63 surface stabilizers, are of particular importance for the protein corona formation. However,
64 the influence of functional groups binding the NP gold core in terms of binding energy is
65 rather poorly reported. Thus, our work aimed at filling the information gap on the influence of
66 the ligand characteristics on AuNP blood compatibility. We hypothesized that this is a key
67 factor that governs the stability of the particles as soon as they are injected into the
68 bloodstream. Besides, the ability of the ligand, to be more or less displaced, induces a
69 selection of the proteins forming the corona. Therefore, the binding energy of the ligand
70 influences the plasmatic mean residence time of the particles and therefore their
71 biodistribution and pharmacokinetics.

72 In this work, we considered that the prediction of AuNP blood compatibility is a
73 multifactorial equation in which the variables are the ligand characteristics (binding energy
74 and charged groups) and the protein characteristics. We synthesized five different types of
75 AuNP with characteristics and ligands frequently described in the biomedical field. Thus,
76 AuNP-citrate, stabilized through weak interactions with carboxylate groups, are often used as
77 precursors for further functionalization steps through ligand exchange. AuNP stabilized by
78 poly(allylamine) (PAH), a cationic polymer carrying primary amines able to bound the
79 particle gold core were selected as models of positive nanoparticles with a weak ligand. AuNP
80 stabilized by a cationic polymer can be used to create multilayered coated particles for a drug
81 delivery purpose (Reum et al., 2010). We also selected AuNP capped by a ligand carrying one
82 or more thiols. Positively charged particles were obtained with cysteamine. Here, the

83 interaction with the gold core was predominantly driven by the thiol group thanks to sulfur
84 atom avidity for gold largely greater than the one between amine and gold. PEG capping
85 allowed the synthesis of neutral particles and it is the gold standard for giving a protein
86 antifouling ability to AuNP. Herein, a PEG bearing two thiol groups was chosen for better
87 anchoring of the ligand on the gold core (Zopes et al., 2013). This also allowed the formation
88 of looped PEG chains on the AuNP, which are known to have better biocompatibility, salt
89 resilience and enhanced hydrophilicity (Du et al., 2019). AuNP were also synthesized using
90 dihydrolipoic acid (DHLA), providing negatively charged particles with a strongly bound
91 ligand (by two thiols per molecule). DHLA has the advantage of adding a carboxylic acid to
92 AuNP surface allowing an easy functionalization through amide bond formation (Roux et al.,
93 2005).

94 Based on the Vroman's effect, two different proteins were selected: albumin (firstly bound)
95 and fibrinogen (latterly bound) as models (described in Table 1.) for probing AuNP-plasma
96 proteins interaction. We investigated the physicochemical characterization of [AuNP, Protein]
97 complexes as of function of particle charge and ligand binding energy using dynamic light
98 scattering and spectrophotometry. The fluorescence quenching of albumin and fibrinogen at
99 several temperatures and AuNP concentrations was measured. Thermodynamic parameters
100 (Bi et al., 2004) of proteins interacting with anionic, cationic or neutral AuNP were
101 determined. Lastly, the hemolysis induced by AuNP as a function of their characteristics was
102 also probed. Our study showed that not only the particle charge but also the ligand binding
103 energy determine the formation of the protein corona on NP. Those new objects display a
104 different reactivity towards the blood compartment as observed in the hemolysis induction.

105

106

107 2. Materials & Methods

108 2.1 Reagents and standards

109 All reagents and solvents were of analytic grade and were used without further purification.
110 Ultrapure deionized water ($> 18.2 \text{ M}\Omega \text{ cm}$) was used for the preparation of all solutions.
111 Polyallylamine hydrochloride (PAH) with average molecular masse of 17,500, cysteamine
112 hydrochloride, dihydrolipoic acid (DHLA), sodium citrate, di-thiolated polyethylene glycol
113 (PEG) with an average molecular mass of 8000, HAuCl_4 , NaBH_4 , human serum albumin and
114 human fibrinogen were supplied by Sigma Aldrich. Wistar rat whole blood collected in
115 heparin blood collection tubes was provided by our laboratory animal house. Na_2HPO_4 ,
116 KH_2PO_4 , KCl and NaCl were purchased from VWR Chemicals. Phosphate buffer saline
117 solution (PBS) at 0.15 M was prepared as follows: $[\text{Na}_2\text{HPO}_4] = 6.68 \times 10^{-3} \text{ M}$, $[\text{KH}_2\text{PO}_4] =$
118 $1.47 \times 10^{-3} \text{ M}$, $[\text{NaCl}] = 138.00 \times 10^{-3} \text{ M}$, and $[\text{KCl}] = 2.68 \times 10^{-3} \text{ M}$, final pH was adjusted to
119 7.40. 50 nM Human albumin and human fibrinogen were prepared by diluting a 1 μM stock
120 solution in PBS.

121 2.2 AuNP synthesis

122 Citrate stabilized AuNP were synthesized in aqueous solution according to our previous work
123 (Tournebize et al., 2012). Under inert atmosphere, 1 mL of HAuCl_4 solution (10 mg/mL) was
124 added into 90 mL of water and then 2 mL of sodium citrate 55 mM. The solution was stirred
125 for 1 min then 1 mL of NaBH_4 19 mM was added and the solution was stirred for 10 min.
126 AuNP DHLA and PEG were obtained through ligand exchange with previously described
127 AuNP. 10 mL of 60 mM DHLA or dithiolated PEG solutions prepared in NaOH 0.5 M were
128 added to 25 mL of AuNP citrate. After an overnight reaction, AuNP were dialyzed twice
129 against PBS for 24 h. AuNP-PAH were synthesized with the same method as AuNP citrate
130 using 1 mL of 87 mM of PAH solution as stabilizing ligand. AuNP cysteamine were

131 synthesized by a two steps reduction method. At first, 90 mL of ultra-pure water added with 1
132 mL of H_{AuCl₄} solution (10 mg/mL) and 1 mL of cysteamine hydrochloride 27 mM. This
133 solution was heated using a heating sand bath (250 °C) and a reflux system until it becomes
134 colorless, corresponding to Au³⁺ reduction to Au⁺ by thiols. The second reduction Au⁺ to Au⁰
135 was performed by adding 50 μL of 19 mM of NaBH₄. Ionic gold quantification was
136 performed on every synthesis with a previously developed in house method (Pallotta et al.,
137 2018). Synthesis yields were found above 99.6 % for each kind of AuNP.

138 2.3 AuNP characterization

139 Colloidal gold nanoparticles were characterized after synthesis without any dilution step. UV–
140 vis spectrophotometer (UV-1800 Shimadzu) was used for spectra recordings and absorbance
141 measurements. The hydrodynamic diameter in volume mode (D_h) and zeta potential (ζ) of
142 AuNP were measured at 20 ± 1 °C with a backscattering detection angle of 173°. Zeta
143 potential was calculated after the conversion of electrophoretic mobility values measured by
144 laser Doppler velocimetry using the Smoluchowski's equation. Both, DLS and laser Doppler
145 velocimetry measurements were conducted on a Zeta Sizer nanoseries Nano-ZS fitted with a
146 helium-neon laser performing at 633 nm (Malvern Instruments, UK). Transmission Electron
147 Microscopy (TEM) images were recorded using a Philips CM20 instrument with a LaB6
148 cathode at 200 kV and with CF200-CU carbon covered copper grids. DigitalMicrograph
149 software was used to determine AuNP cores diameters, D_c, by measuring at least 150
150 individualized nanoparticles.

151

152 2.4 Interaction of AuNP and proteins studied by spectrophotometry and dynamic light scattering

153 Concentrations of AuNP ranging from (3.5 nM to 21 nM for Citrate, PAH, Cysteamine
154 stabilized AuNP and DHLA, PEG capped AuNP), corresponding to a quantity of 10^{12} to 10^{13}
155 particles per samples were used. AuNP concentrations were comparable to those used in
156 biodistribution studies after intravenous injection. For example, (Zhang et al., 2009) and
157 (Semmler-Behnke et al., 2008) studied AuNP biodistribution in mice and rats after injection
158 of quantities ranging from 1×10^{12} to 9×10^{13} and 4×10^{12} to 4×10^{13} per animals
159 respectively. All AuNP dilutions were prepared in PBS 0.15 M pH = 7.4 containing albumin
160 or fibrinogen with a final concentration of 50 nM. Visible spectra (400 – 800 nm) and
161 hydrodynamic diameters were acquired just after mixing at 20 ± 1 °C. Results are reported as
162 the main hydrodynamic diameters measured in volume. External layer thickness (sum of the
163 ligand layer, the protein corona and the solvation shell) was determined by subtracting the
164 AuNP D_c to the D_h of [AuNP, Protein] complexes.

165 2.5 Fluorescence quenching study and constants determinations.

166 The analysis of AuNP and proteins interaction was performed through fluorescence quenching
167 experiments as a function of temperature (4 °C, 20 °C, 37°C and 50 °C) and AuNP
168 concentration (3.5 nM to 21 nM). Albumin and fibrinogen concentrations were kept constant
169 (50 nM). This concentration was chosen greater than AuNP concentration and with a
170 sufficient fluorescence signal for quenching studies. Proteins solutions, PBS and AuNP were
171 pre-incubated at 4 °C, 20 °C, 37°C or 50 °C before mixing and measurements. The
172 fluorescence intensity was measured immediately after sample preparation using a quartz
173 cuvette with a light path 10x4 mm (Hellma Analytics, Müllheim, Germany). Hitachi F-2000
174 Fluorescence Spectrophotometer equipped with a Xenon lamp and with a temperature-
175 controlled analysis chamber was used to perform the assay. The excitation and emission

176 wavelengths were set at 280 ± 5 nm and 340 ± 5 nm, respectively. Sensitivity was set in high
177 mode for albumin conditions and on medium for fibrinogen.

178 The protein fluorescence quenching relied on the interaction of albumin or fibrinogen with
179 AuNP assimilated to a ligand according to the following equation (1):



181
182 K_a being the affinity constant. For referring to the formation of this complex, in the text the
183 following notation was used [AuNP-X/@X, albumin or fibrinogen], where -X or @X
184 represent the stabilizing or capping ligand under consideration, respectively.

185

186 The fluorescence quenching mechanism was determined with the Stern-Volmer equation (2):

187
$$\frac{F_0}{F} = 1 + K_q \tau_0 [AuNP] = 1 + K_{SV} [AuNP] \quad (2)$$

188 In which, F_0 and F are the fluorescence intensities of albumin or fibrinogen in the absence and
189 presence of quencher (AuNP), respectively. K_{SV} is the Stern-Volmer quenching constant, K_q
190 the quenching constant, $[AuNP]$ the molar concentration of AuNP and τ_0 is the lifetime of
191 albumin and fibrinogen without quencher, which was considered as 10^{-7} s.

192 Static quenching allows the calculation of affinity constant (Ka) and Hill coefficient (n) with
193 the following equation (3):

194
$$\log \frac{F_0 - F}{F} = \log Ka + n \log [AuNP] \quad (3)$$

195 Previously mentioned constants were determined by plotting $\log \frac{F_0 - F}{F}$ versus $\log [AuNP]$.
196 Slopes and intercepts of the resulting curves represented Hill coefficient and
197 $\log Ka$ respectively.

198
199 Entropy (ΔS) and enthalpy (ΔH) variations were determined with the Van't Hoff model.
200 Previously mentioned constants were determined by plotting $\ln Ka$ as a function of $\frac{1}{T}$, where
201 T is the temperature in K.

202 Slopes and intercepts of the resulting curves respectively represented $\frac{-\Delta H}{R}$ and $\frac{\Delta S}{R}$.

203 R being the perfect gas constant taken equal to $8.314 \text{ J.K}^{-1}.\text{mol}^{-1}$.

204

205

206 Gibbs free energy (ΔG) was calculated with the following equation (4):

207
$$\Delta G = -RT \ln Ka \quad (4)$$

208 2.6 AuNP induced hemolysis

209 AuNP ability to induce hemolysis was adapted from a previously described method (Pallotta
210 et al., 2017) using blood from a Wistar male rat. Briefly, Red Blood Cells (RBC) washing was
211 performed after centrifugation (20 min, 3000 rpm, 4 °C) by substituting the plasma by the
212 same volume of NaCl 0.9 % (m/v). A stock solution was prepared by mixing 1 mL of
213 previously described RBC solution and 1.25 mL of NaCl 0.9 % (W/V). Working solutions
214 were obtained by a 25-fold dilution on PBS alone, with albumin or fibrinogen. Positive and
215 negative controls were obtained through the same dilutions in ultra-pure water or PBS,
216 respectively. Protein (albumin and fibrinogen) final concentration was 50 nM and AuNP
217 concentration ranged from 3.5 to 21 nM. PBS was preferred instead of NaCl 0.9 % to ensure
218 the same proteins protonation state as *in vivo*. Samples were prepared in triplicates and
219 incubated in a shaking and heating water bath (80 oscillations.min⁻¹ and 37 °C) during 2 h.
220 The hemolysis rate was determined by measuring the absorbance of the samples at $\lambda = 541$
221 nm after centrifugation (10 min, 5 000 rpm). Hemolysis rates induced by AuNP were
222 expressed as a percentage of the hemolysis found with the positive control.

223

224 3. Results and Discussion

225 3.1 Nanoparticles characterization

226 Several types of gold nanoparticles were synthesized using stabilization agent of various
227 chemical nature with increasing binding energy for Au core: carboxylate groups for citrate
228 ions, amine groups for PAH, thiol groups for cysteamine and dithiol groups for DHLA and
229 PEG. Their physicochemical characterization was performed, and the results are presented in
230 Table 2. and Figure 1. Spectrophotometric properties of these particles showed a single
231 plasmon band (λ_{\max}) characteristic of metallic nanoparticles. No other peak was detected,
232 meaning that little to none aggregation was observed. This was confirmed by transmission
233 electron microscopy observations that showed spherical and individualized particles.
234 Hydrodynamic diameters (D_h) and core diameters (D_c) measurement allowed the
235 determination of AuNP stabilization and solvation layers thickness. The use of different
236 ligands during synthesis provided negatively charged NP (AuNP-Citrate and @DHLA), or
237 neutral particles (AuNP@PEG) or positively charged NP (AuNP-PAH and @Cysteamine)

238 3.2 Protein effect on AuNP physicochemical characterization

239 Albumin and fibrinogen were selected as models for studying the interaction of AuNP with
240 blood proteins. Albumin is known to be a ubiquitous carrier able to rapidly bound on NP. In a
241 second step, this non-specific binding is replaced by complexation with other more
242 specialized blood proteins such as fibrinogen corresponding to the Vroman's effect. The study
243 of the physicochemical characterization of AuNPs in the presence of these two proteins
244 represents a first step towards understanding the fate of AuNP in blood.

245

246 3.2.1 Modification of AuNP optical properties

247 The interaction of [AuNP, Protein] and its effect on their optical properties were studied by
248 visible spectrophotometry (Figure 2.). Variation of the Surface Plasmon Band was studied by
249 mixing an increasing concentration of AuNP with a constant concentration (50 nM) of either
250 albumin or fibrinogen. This physicochemical parameter is specific to metallic nanoparticles
251 and gives information on their size, their form, their surrounding medium, and neighbors
252 particularly the inter-nanoparticulate distance (Amendola et al., 2017). As reported in the
253 histograms a redshift of the plasmon band was observed, corresponding to NP surrounding
254 modification due to proteins. The highest increases in maximal wavelength were observed for
255 citrate, PAH and cysteamine AuNP (Figure 2. A, B, C) reflecting a significant impact on the
256 physicochemical properties of these particles after protein binding. Plasmon band broadening
257 was related to an increase of AuNP size dispersion (Moore and Goettmann, 2006) due to the
258 formation of a protein corona around them and/or to the formation of aggregates. For DHLA
259 and PEG AuNP (Figure 2. E, F) these changes were less pronounced representing a limited
260 impact of proteins on these particles.

261

262 3. 2.2 Variation of AuNP Dh induced by proteins

263 The variation of Dh as a function of AuNP concentration with either albumin or fibrinogen
264 was probed (Figure 3.). Differences between AuNP Dc and Dh gave an estimation of the
265 surrounding layer thickness. This external layer thickness was defined as the sum of the
266 ligand layer, the protein corona and the solvation shell. It was calculated only when particles
267 were not aggregated. Values of typical diameters measured or estimated at AuNP
268 concentration of 7 nM are listed in Table 3. AuNP-citrate Dh were found more important in
269 presence of albumin than without. Still, for this kind of AuNP, the Dh stayed stable at any NP
270 concentration, suggesting the formation of a stable protein corona on individualized particles.
271 At the opposite, as far as AuNP-citrate are concerned, the formation of increasingly important
272 aggregates was observed in the presence of fibrinogen. For PAH stabilized nanoparticles large
273 aggregates over 500 nm were observed in both protein conditions at any AuNP concentrations
274 revealing an important instability of these particles in a biological-like medium.
275 Hydrodynamic diameters of cysteamine nanoparticles increased gradually for both albumin
276 and fibrinogen conditions, highlighting an aggregation mediated by AuNP concentration.
277 Fibrinogen tendency to form large aggregates or to induce the formation of thicker corona
278 compared to albumin is due to its shape and dimensions (Table 1.), in fact, this protein is able
279 to bridge several nanoparticles or to be organized as a loop on a single particle (Deng et al.,
280 2012). Hydrodynamic diameters of DHLA and PEG particles were found to be stable over the
281 whole range of the studied AuNP concentration.

282 3.3. Mechanism of AuNP binding to protein

283 As reported in Table 1, albumin and fibrinogen both carry tryptophan residues which
284 fluorescence can be quenched as a function of the presence of various compounds. Then, a
285 thorough characterization of AuNP-protein interactions was allowed through fluorescence

286 study. Thermodynamics parameters, quenching, K_{SV} , and affinity, K_a , constants were
287 determined for both proteins and as a function of AuNP surface ligands.

288

289 3.3.1. Quenching constants

290 Fluorescence quenching studies relied on the native fluorescence (F_0) of proteins mainly
291 carried by tryptophan residues. The addition of molecules or particles able to bind on protein
292 induces a fluorescence quenching. Then, a decreasing fluorescence intensity (F) was observed
293 when AuNP concentration was increased. Plotting of F_0/F as a function of AuNP
294 concentrations (Figure 4.) allowed the determination of Stern-Volmer constant (K_{SV}) for
295 albumin and fibrinogen. In all the studied conditions, the quenching rate constant (K_q) was
296 greater than the maximum diffusion collision quenching rate constant ($2 \times 10^{10} \text{ L.mol}^{-1} .\text{s}^{-1}$
297 (Bi et al., 2004)) meaning that the fluorescence quenching relied on the formation of a static
298 complexes ([AuNP, Albumin] and [AuNP, Fibrinogen]). For a static quenching, the
299 interaction site between AuNP and protein is located in the close vicinity (between 10 \AA and
300 100 \AA (Swathi and Sebastian, 2009)) of the fluorophores (tryptophan) and the distance
301 between protein and quencher stays constant, on the contrary to a collisional or dynamic
302 complex.

303 3.3.2 Thermodynamics constants of AuNP proteins interaction

304 Plotting of $\log \frac{F_0 - F}{F}$ as a function of $\log[AuNP]$ values at $37 \text{ }^\circ\text{C}$ (Figure 5.) gave the
305 parameters listed in Table 5. Hill coefficient can also be defined as a measure of binding
306 cooperativity. The value lower than 1 obtained for [AuNP@DHLA, Albumin] corresponds to
307 an anticooperative binding indicating that the association energy per particle progressively
308 decreases with further protein adsorption. For AuNP citrate, PAH, cysteamine, Hill

309 coefficient was found greater than 1 meaning that their interaction with either albumin or
310 fibrinogen relied on a cooperative binding. The association energy increases gradually as long
311 as particles bind on proteins. In the case of [AuNP@DHLA, Fibrinogen] and [AuNP@PEG,
312 Fibrinogen], Hill coefficient was equal to 1 indicating that the association energy of these
313 complexes was not varying as a function of protein adsorption. Besides, ΔG negative values
314 revealed a spontaneous formation of all the [AuNP, Protein] complexes. Affinity constant
315 (K_a) was found greater than 10^3 (excepted for [AuNP@DHLA, Albumin]), indicating a high
316 affinity between each type of AuNP and either albumin or fibrinogen. In the case of the
317 [AuNP@DHLA, Albumin], a low K_a value was found, suggesting a moderate affinity for the
318 complex formation.

319 Entropy and enthalpy variations signs and values (ΔS and ΔH , respectively) allowed the
320 determination of the types of chemical interactions between AuNP and proteins. The negative
321 ΔS and ΔH values obtained for [AuNP-citrate, Albumin], [AuNP-PAH, Albumin],
322 [AuNP@cysteamine, Albumine], [AuNP@DHLA, Albumin] and [AuNP-PAH, Fibrinogen]
323 are characteristics of an interaction based on Van der Waals and/or H-bond formation. These
324 weak energy interactions are frequently managing contacts between particles and
325 biomolecules. They allow stabilizing interactions between the solvating layers of each object
326 as well as between their respective surfaces. The positive values of ΔS and ΔH are linked to
327 hydrophobic interactions. A positive ΔS and a positive or negative value for ΔH indicate an
328 ionic interaction. In this context, definitions of these two forces are important to understand
329 the precise nature of the interactions leading to the complex formation. Hydrophobic
330 association (Ross and Subramanian, 1981) is exclusively referring to the partial withdrawal of
331 a nonpolar group from water and/or from the solvation layers of AuNP or proteins and not to
332 an interaction between nonpolar groups themselves. The ionic association represents a
333 neutralization of opposite charges (Manning, 1978). Here, the scale at which this interaction

334 occurs is an important consideration. This must be understood as an electrostatic interaction
335 between the particle and the protein and not between two net charges present on the different
336 objects. Considering those definitions, hydrophobic and ionic interactions found for
337 [AuNP@PEG, Albumin], [AuNP-citrate, Fibrinogen] and [AuNP@cysteamine, Fibrinogen]
338 relied on the modification of the species (non-polar and charged groups or ions) involved in
339 the solvation layers of AuNP and the protein resulting from the association. The ionic
340 association found for [AuNP@DHLA, Fibrinogen] is based on the interaction of negatively
341 charged AuNP@DHLA (carboxylate groups) and positively charged residues of fibrinogen.
342 Concerning [AuNP@PEG, Fibrinogen] an analogous phenomenon explains the ionic
343 interaction found. it has already been described that a PEG capping layer does not offer a total
344 screening of charge(Wang et al., 2013) carried by the particle gold core. In the case of
345 AuNP@PEG, the electron cloud of the core may stay mobilizable for electrostatic
346 interactions.

347 3.4 AuNP interaction with blood

348 AuNP were incubated with RBC without (Figure 6. A) or with albumin (Figure 6. B) and
349 fibrinogen (Figure 6. C) to probe their ability to induce hemolysis. For each condition and all
350 AuNP types, hemolysis was found increasing as a function of AuNP concentration.

351 In the first condition without protein (Figure 6. A), two opposite behaviors were identified.
352 Citrate and PAH stabilized and cysteamine capped AuNP induced a significant level of
353 hemolysis greater than 10 % from the lowest concentration. The mechanisms explaining these
354 results are based on AuNP surface ligands. It is commonly known that citrate ions with the
355 lowest binding energy for NP gold core (Table 2) are forming an easily displaceable shell.
356 These particles strongly interacted with RBC through ligand exchange with their membrane
357 components such as sialic acid. On the other side, cysteamine, a strongly bound ligand, could

358 not be removed. These positively charged NP interacted with negatively charged RBC
359 membranes through electrostatic interactions. PAH, an intermediate strength ligand between
360 carboxylic acid and thiol reacted through a combination of ligand exchange and charge
361 interaction. Whereas for DHLA and PEG capped AuNP, hemolysis greater than 10 % was
362 generated only at the highest concentration. Here, those particles are capped by non-
363 displaceable ligands carrying two thiols. The low hemolysis rate found also relied on the
364 negative charge of AuNP@DHLA and the steric hindrance provided by AuNP@PEG. Here,
365 AuNP induced hemolysis was driven by two factors, ligand binding energy and the particle
366 charge.

367 Addition of either albumin (figure 6. B) or fibrinogen (Figure 6. C) during the assay revealed
368 a protein influence on the AuNP induced hemolysis. Considering the previous results showing
369 the spontaneous formation of the static complex [AuNP, Protein], hemolysis should now be
370 considered as being generated by new objects resulting from this association. The two
371 previously described behaviors were still found. Concerning citrate and PAH stabilized AuNP
372 and cysteamine capped AuNP at a concentration greater than 7 nM, hemolysis was found
373 increased in presence of the proteins. The positive binding cooperativity (Hill coefficient, n
374 >1) certainly promoted the interaction between the [AuNP, Protein] complexes and RBC.
375 Furthermore, for those particles, the hemolysis ratio was more important with fibrinogen. This
376 could be explained by the strongest affinity constants (K_a) and higher positive binding
377 cooperativities found for fibrinogen compared to albumin, leading to the formation of larger
378 aggregates.

379 On the other hand, hemolysis generated by [AUNP@DHLA, Albumin], [AUNP@DHLA,
380 Fibrinogen], [AUNP@PEG, Albumin] and [AUNP@PEG, Fibrinogen] complexes was lower
381 than the one induced by the 3 others particles. The values were not significantly different

382 from the negative control at low AuNP concentration. Even if the formation of static
383 complexes between those particles and proteins has been identified, spectrophotometric and
384 dynamic light scattering studies demonstrated a limited modification of AuNP
385 physicochemical parameters induced by proteins. Fluorescence quenching gave Hill
386 coefficient values less than or equal to one, suggesting that protein corona surrounding
387 AuNP@DHLA and AuNP@PEG did not promote the interaction of [AUNP@DHLA,
388 Albumin], [AUNP@DHLA, Fibrinogen], [AUNP@PEG, Albumin] and [AUNP@PEG,
389 Fibrinogen] complexes with RBC.

390 Taken altogether, these results fully described [AuNP, Protein] complexes interaction. Indeed,
391 the influence of proteins on nanoparticle characterization was probed through
392 spectrophotometric and dynamic light scattering studies. An important modification of citrate
393 and PAH stabilized and cysteamine capped AuNP physicochemical parameters was observed
394 in the presence of proteins. Weakly stabilized citrate AuNP remained in the nanoparticle form
395 with albumin but were aggregated with fibrinogen, showing that the protein nature is also an
396 important parameter (Zhang et al., 2014). Also, this study points out that working on solely
397 albumin represents a limited model for the study of protein - nanoparticle interaction.
398 Positively charged AuNP (PAH and cysteamine) formed aggregates with either albumin or
399 fibrinogen. Other studies have already shown such results. For example, it has been
400 demonstrated that cetyltrimethylammonium bromide (CTAB) stabilized AuNP aggregate with
401 albumin through electrostatic interactions (Boulos et al., 2013; Wang et al., 2019). Besides,
402 we showed here, that this aggregation also depends on the binding energy of the AuNP
403 surface ligands. Impact of the nanoparticles on the native fluorescence of proteins allowed
404 quenching studies and the determination thermodynamics constants describing those
405 interactions. It has been shown that the corona protein formation on AuNP is a dynamic
406 phenomenon responding to the Vroman's effect. At first, AuNP interact with unspecialized

407 protein such as albumin and then, they tend to be bound by other more specialized proteins. In
408 this study, a higher affinity was found between all particles and fibrinogen rather than
409 albumin. We also demonstrated that this affinity depends on the nature of the AuNP surface
410 ligand. Lastly, many studies described the formation of protein corona on AuNP as a function
411 of protein nature, of NP hydrodynamic diameter (Xiao et al., 2018) or medium conditions
412 such as pH (Sotnikov et al., 2019). The conditions of corona formation, its evolution over
413 time or its impact on the bioavailability of nanoparticles were previously published. In this
414 work, we proved that hemolysis can be strengthened by the formation of this protein corona
415 and to the best of our knowledge this article is the first to report this behavior.

416 Conclusion

417 Pulled together, our results drew up of the composite sketch of an ideal surface ligand for
418 blood compatibles AuNP. The best capping agent should be strongly bound to the gold core
419 by one or more thiols group and it must confer a negative charge to the particles.

420 Further studies are still required to fully describe the influence of AuNP surface ligand in the
421 interaction with the blood compartment. Our future works will focus on AuNP effect on the
422 coagulation and the inflammatory response. Indeed, thrombin activation as a function of
423 AuNP nature or with the proteins of the complement pathway will be studied.

424

425 Acknowledgments

426 Authors thank laboratory animal house (ACBS) for providing rat whole blood. The authors

427 also acknowledge “Region Grand Est” for financial support.

428 Declarations of interest: none

429

430 References

- 431 Al-Johani, H., Abou-Hamad, E., Jedidi, A., Widdifield, C.M., Viger-Gravel, J., Sangaru, S.S.,
432 Gajan, D., Anjum, D.H., Ould-Chikh, S., Hedhili, M.N., Gurinov, A., Kelly, M.J., El
433 Eter, M., Cavallo, L., Emsley, L., Basset, J.-M., 2017. The structure and binding mode
434 of citrate in the stabilization of gold nanoparticles. *Nat. Chem.* 9, 890–895.
435 <https://doi.org/10.1038/nchem.2752>
- 436 Amendola, V., Pilot, R., Frasconi, M., Maragò, O.M., Iatì, M.A., 2017. Surface plasmon
437 resonance in gold nanoparticles: a review. *J. Phys. Condens. Matter* 29, 203002.
438 <https://doi.org/10.1088/1361-648X/aa60f3>
- 439 Bi, S., Ding, L., Tian, Y., Song, D., Zhou, X., Liu, X., Zhang, H., 2004. Investigation of the
440 interaction between flavonoids and human serum albumin. *J. Mol. Struct.* 703, 37–45.
441 <https://doi.org/10.1016/j.molstruc.2004.05.026>
- 442 Boulos, S.P., Davis, T.A., Yang, J.A., Lohse, S.E., Alkilany, A.M., Holland, L.A., Murphy,
443 C.J., 2013. Nanoparticle–Protein Interactions: A Thermodynamic and Kinetic Study of
444 the Adsorption of Bovine Serum Albumin to Gold Nanoparticle Surfaces. *Langmuir*
445 29, 14984–14996. <https://doi.org/10.1021/la402920f>
- 446 Cieśla, M., Adamczyk, Z., Barbasz, J., Wasilewska, M., 2013. Mechanisms of Fibrinogen
447 Adsorption at Solid Substrates at Lower pH. *Langmuir* 29, 7005–7016.
448 <https://doi.org/10.1021/la4012789>
- 449 Daniel, M. C., & Astruc, D. (2004). Gold nanoparticles: Assembly, supramolecular chemistry,
450 quantum-size-related properties, and applications toward biology, catalysis, and
451 nanotechnology. *Chemical Reviews*, 104(1), 293–346.
452 <https://doi.org/10.1021/cr030698+>

453 Deng, Z.J., Liang, M., Toth, I., Monteiro, M.J., Minchin, R.F., 2012. Molecular Interaction of
454 Poly(acrylic acid) Gold Nanoparticles with Human Fibrinogen. *ACS Nano* 6, 8962–
455 8969. <https://doi.org/10.1021/nn3029953>

456 Du, Y., Jin, J., Liang, H., Jiang, W., 2019. Structural and Physicochemical Properties and
457 Biocompatibility of Linear and Looped Polymer-Capped Gold Nanoparticles.
458 *Langmuir* [acs.langmuir.9b00045](https://doi.org/10.1021/acs.langmuir.9b00045). <https://doi.org/10.1021/acs.langmuir.9b00045>

459 Erickson, H.P., 2009. Size and Shape of Protein Molecules at the Nanometer Level
460 Determined by Sedimentation, Gel Filtration, and Electron Microscopy. *Biol. Proced.*
461 *Online* 11, 32–51. <https://doi.org/10.1007/s12575-009-9008-x>

462 Gonçalves, S., Santos, N.C., Martins-Silva, J., Saldanha, C., 2007. Fluorescence spectroscopy
463 evaluation of fibrinogen– β -estradiol binding. *J. Photochem. Photobiol. B* 86, 170–176.
464 <https://doi.org/10.1016/j.jphotobiol.2006.09.001>

465 Lacerda, S.H.D.P., Park, J.J., Meuse, C., Pristiniski, D., Becker, M.L., Karim, A., Douglas,
466 J.F., 2010. Interaction of Gold Nanoparticles with Common Human Blood Proteins.
467 *ACS Nano* 4, 365–379. <https://doi.org/10.1021/nn9011187>

468 Manning, G.S., 1978. The molecular theory of polyelectrolyte solutions with applications to
469 the electrostatic properties of polynucleotides. *Q. Rev. Biophys.* 11, 179–246.
470 <https://doi.org/10.1017/S0033583500002031>

471 Mieszawska, A.J., Mulder, W.J.M., Fayad, Z.A., Cormode, D.P., 2013. Multifunctional Gold
472 Nanoparticles for Diagnosis and Therapy of Disease. *Mol. Pharm.* 10, 831–847.
473 <https://doi.org/10.1021/mp3005885>

474 Moores, A., Goettmann, F., 2006. The plasmon band in noble metal nanoparticles: an
475 introduction to theory and applications. *New J. Chem.* 30, 1121.
476 <https://doi.org/10.1039/b604038c>

477 Nuzzo, R.G., Zegarski, B.R., Dubois, L.H., 1987. Fundamental Studies of the Chemisorption
478 of Organosulfur Compounds on Au(111). Implications for Molecular Self-Assembly
479 on Gold Surfaces. *J. Am. Chem. Soc.* 109, 733–740.

480 Pallotta, A., Parent, M., Clarot, I., Luo, M., Borr, V., Dan, P., Decot, V., Menu, P., Safar, R.,
481 Joubert, O., Leroy, P., Boudier, A., 2017. Blood Compatibility of Multilayered
482 Polyelectrolyte Films Containing Immobilized Gold Nanoparticles. *Part. Part. Syst.*
483 *Charact.* 34, 1600184. <https://doi.org/10.1002/ppsc.201600184>

484 Pallotta, A., Philippe, V., Boudier, A., Leroy, P., Clarot, I., 2018. Highly sensitive and simple
485 liquid chromatography assay with ion-pairing extraction and visible detection for
486 quantification of gold from nanoparticles. *Talanta* 179, 307–311.
487 <https://doi.org/10.1016/j.talanta.2017.11.016>

488 Purohit, R., Vallabani, N.S., Shukla, R.K., Kumar, A., Singh, S., 2016. Effect of gold
489 nanoparticle size and surface coating on human red blood cells. *Bioinspired Biomim.*
490 *Nanobiomaterials* 5, 121–131. <https://doi.org/10.1680/jbibn.15.00018>

491 Quach, Q.H., Kah, J.C.Y., 2017. Non-specific adsorption of complement proteins affects
492 complement activation pathways of gold nanomaterials. *Nanotoxicology* 11, 382–394.
493 <https://doi.org/10.1080/17435390.2017.1306131>

494 Reum, N., Fink-Straube, C., Klein, T., Hartmann, R.W., Lehr, C.-M., Schneider, M., 2010.
495 Multilayer Coating of Gold Nanoparticles with Drug–Polymer Coadsorbates.
496 *Langmuir* 26, 16901–16908. <https://doi.org/10.1021/la103109b>

497 Ross, P.D., Subramanian, S., 1981. Thermodynamics of protein association reactions: forces
498 contributing to stability. *Biochemistry* 20, 3096–3102.
499 <https://doi.org/10.1021/bi00514a017>

500 Roux, S., Garcia, B., Bridot, J.-L., Salomé, M., Marquette, C., Lemelle, L., Gillet, P., Blum,
501 L., Perriat, P., Tillement, O., 2005. Synthesis, Characterization of Dihydrolipoic Acid

502 Capped Gold Nanoparticles, and Functionalization by the Electroluminescent
503 Luminol. *Langmuir* 21, 2526–2536. <https://doi.org/10.1021/la048082i>

504 Semmler-Behnke, M., Kreyling, W.G., Lipka, J., Fertsch, S., Wenk, A., Takenaka, S., Schmid,
505 G., Brandau, W., 2008. Biodistribution of 1.4- and 18-nm gold particles in rats. *Small*,
506 4, 2108–2111. <https://doi.org/10.1002/sml.200800922>

507 Shemetov, A.A., Nabiev, I., Sukhanova, A., 2012. Molecular Interaction of Proteins and
508 Peptides with Nanoparticles. *ACS Nano* 6, 4585–4602.
509 <https://doi.org/10.1021/nn300415x>

510 Sotnikov, D.V., Berlina, A.N., Ivanov, V.S., Zherdev, A.V., Dzantiev, B.B., 2019. Adsorption
511 of proteins on gold nanoparticles: One or more layers? *Colloids Surf. B Biointerfaces*
512 173, 557–563. <https://doi.org/10.1016/j.colsurfb.2018.10.025>

513 Swathi, R.S., Sebastian, K.L., 2009. Distance dependence of fluorescence resonance energy
514 transfer. *J. Chem. Sci.* 121, 777–787. <https://doi.org/10.1007/s12039-009-0092-x>

515 Tournebize, J., Boudier, A., Sapin-Minet, A., Maincent, P., Leroy, P., Schneider, R., 2012.
516 Role of Gold Nanoparticles Capping Density on Stability and Surface Reactivity to
517 Design Drug Delivery Platforms. *ACS Appl. Mater. Interfaces* 4, 5790–5799.
518 <https://doi.org/10.1021/am3012752>

519 Vroman, L., 1962. Effect of absorbed proteins on the wettability of hydrophilic and
520 hydrophobic solids. *Nature* 196, 476–477. <https://doi.org/10.1038/196476a0>

521 Wang, G., Yan, C., Gao, S., Liu, Y., 2019. Surface chemistry of gold nanoparticles
522 determines interactions with bovine serum albumin. *Mater. Sci. Eng. C* 103, 109856.
523 <https://doi.org/10.1016/j.msec.2019.109856>

524 Wang, P., Wang, X., Wang, L., Hou, X., Liu, W., Chen, C., 2015. Interaction of gold
525 nanoparticles with proteins and cells. *Sci. Technol. Adv. Mater.* 16, 034610.
526 <https://doi.org/10.1088/1468-6996/16/3/034610>

527 Wang, W., Wei, Q.-Q., Wang, J., Wang, B.-C., Zhang, S., Yuan, Z., 2013. Role of thiol-
528 containing polyethylene glycol (thiol-PEG) in the modification process of gold
529 nanoparticles (AuNPs): Stabilizer or coagulant? *J. Colloid Interface Sci.* 404, 223–
530 229. <https://doi.org/10.1016/j.jcis.2013.04.020>

531 Xiao, W., Xiong, J., Zhang, S., Xiong, Y., Zhang, H., Gao, H., 2018. Influence of ligands
532 property and particle size of gold nanoparticles on the protein adsorption and
533 corresponding targeting ability. *Int. J. Pharm.* 538, 105–111.
534 <https://doi.org/10.1016/j.ijpharm.2018.01.011>

535 Xie, X., Liao, J., Shao, X., Li, Q., Lin, Y., 2017. The Effect of shape on Cellular Uptake of
536 Gold Nanoparticles in the forms of Stars, Rods, and Triangles. *Sci. Rep.* 7, 3827.
537 <https://doi.org/10.1038/s41598-017-04229-z>

538 Zhang, G., Yang, Z., Lu, W., Zhang, R., Huang, Q., Tian, M., Li, L.,
539 Liang D., Li, C., 2009. Influence of anchoring ligands and particle size on the colloidal
540 stability and in vivo biodistribution of polyethylene glycol-coated gold nanoparticles
541 in tumor-xenografted mice. *Biomaterials* 30, 1928–1936.
542 <https://doi.org/10.1016/j.biomaterials.2008.12.038>

543 Zhang, S., Moustafa, Y., Huo, Q., 2014. Different Interaction Modes of Biomolecules with
544 Citrate-Capped Gold Nanoparticles. *ACS Appl. Mater. Interfaces* 6, 21184–21192.
545 <https://doi.org/10.1021/am506112u>

546 Zopes, D., Stein, B., Mathur, S., Graf, C., 2013. Improved Stability of “Naked” Gold
547 Nanoparticles Enabled by in Situ Coating with Mono and Multivalent Thiol PEG
548 Ligands. *Langmuir* 29, 11217–11226. <https://doi.org/10.1021/la4012058>
549

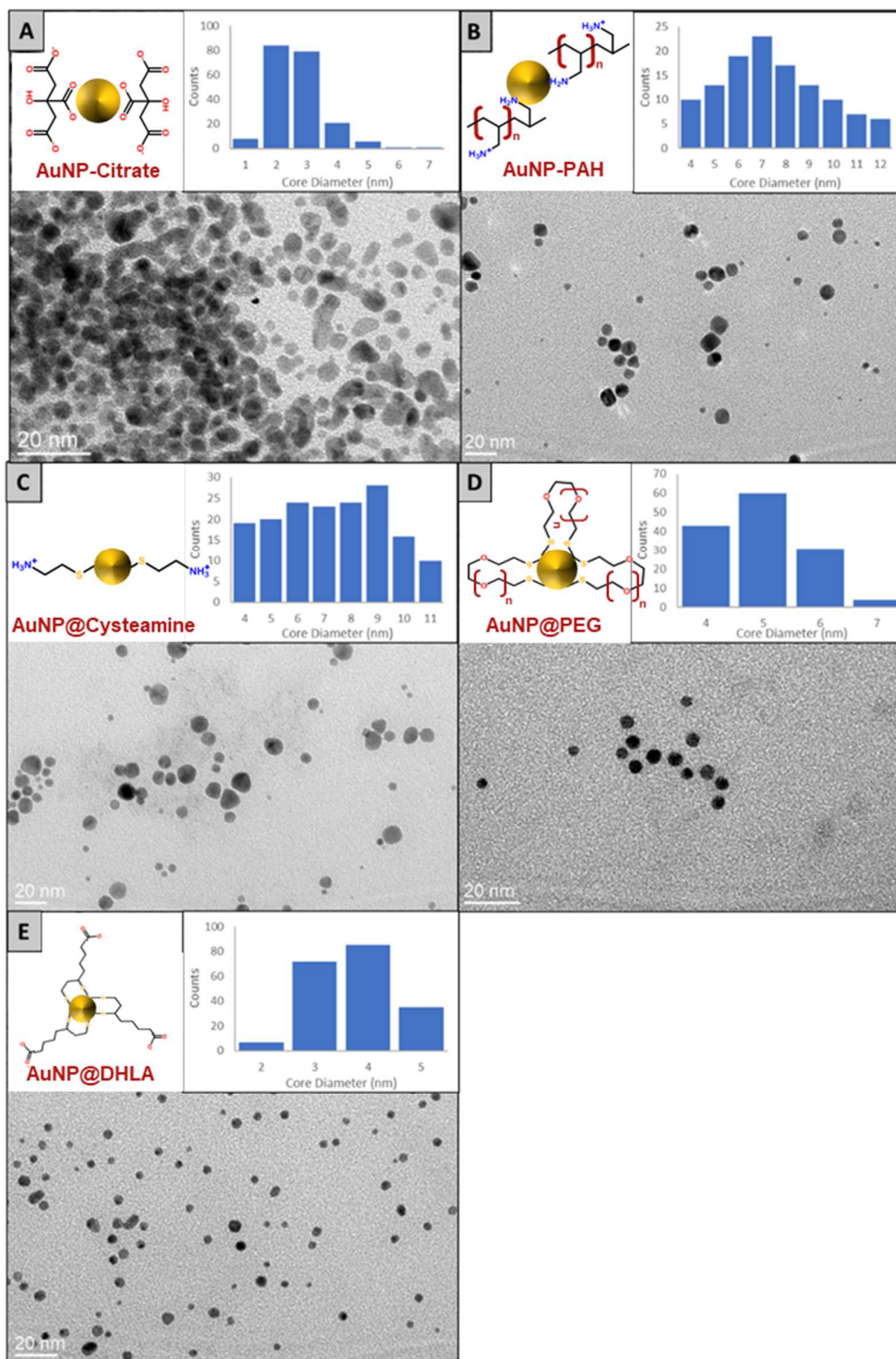


Figure 1. Observation by TEM of AuNP stabilized by citrate (A), PAH (B), capped by cysteamine (C), DHHLA (D) and PEG (E) and histograms representing AuNP Dc measured on at least 150 individualized particles. Schematic representations of the studied nanoparticles are also represented.

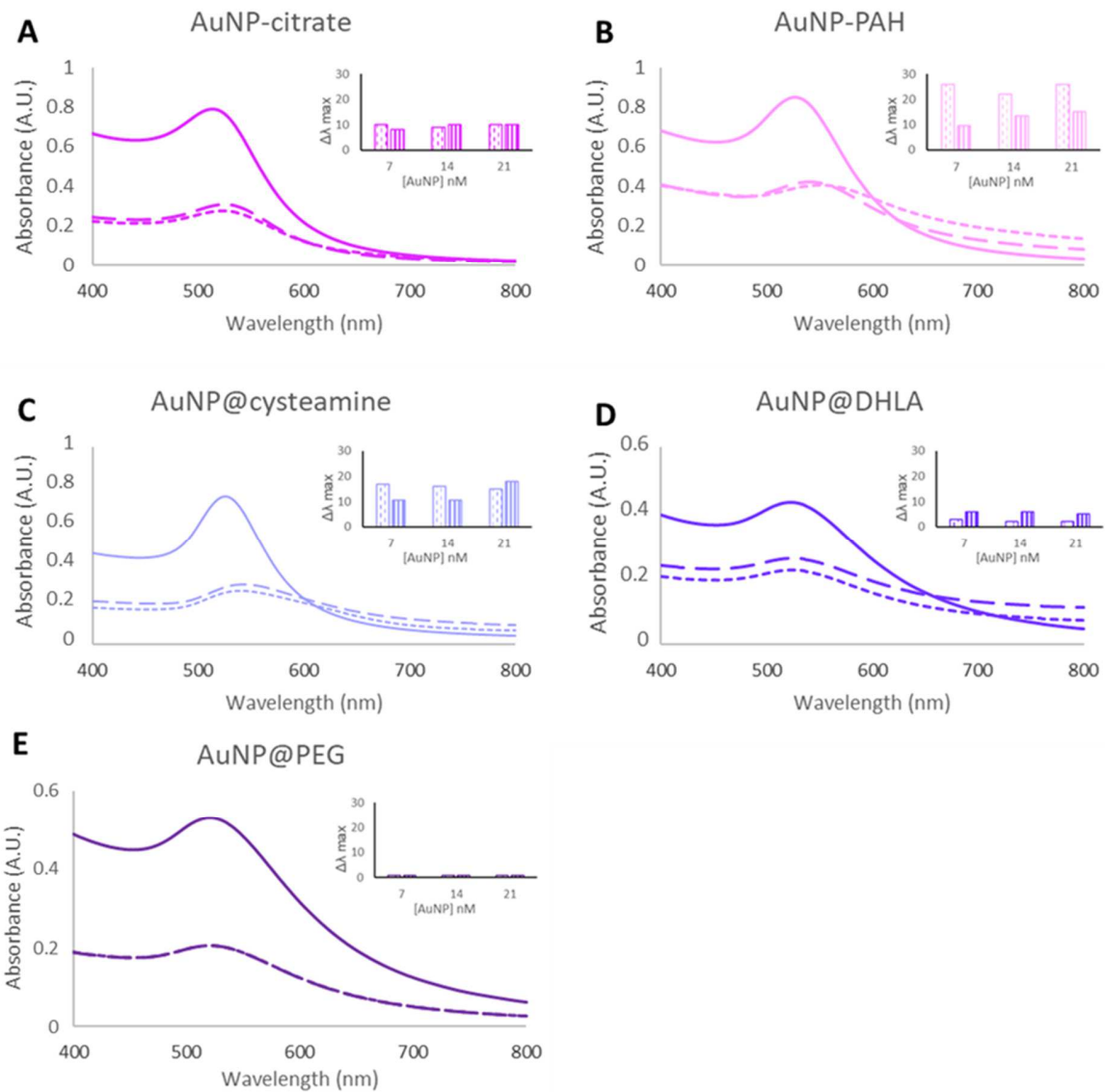


Figure 2. Typical visible spectra of citrate, PAH, cysteamine AuNP(A,B,C) at 70 nM and DHLA, PEG AuNP at 50 nM (solid line) and spectra of AuNP (21 nM) mixed with either albumin (short dashed lines) or fibrinogen (long dashed lines) at 50 nM. Histograms represent the variation of the Surface Plasmon Band wavelength after mixing AuNP (at 7, 14, and 21 nM) with albumin (short dashed) or fibrinogen (long dashed) at 50 nM.

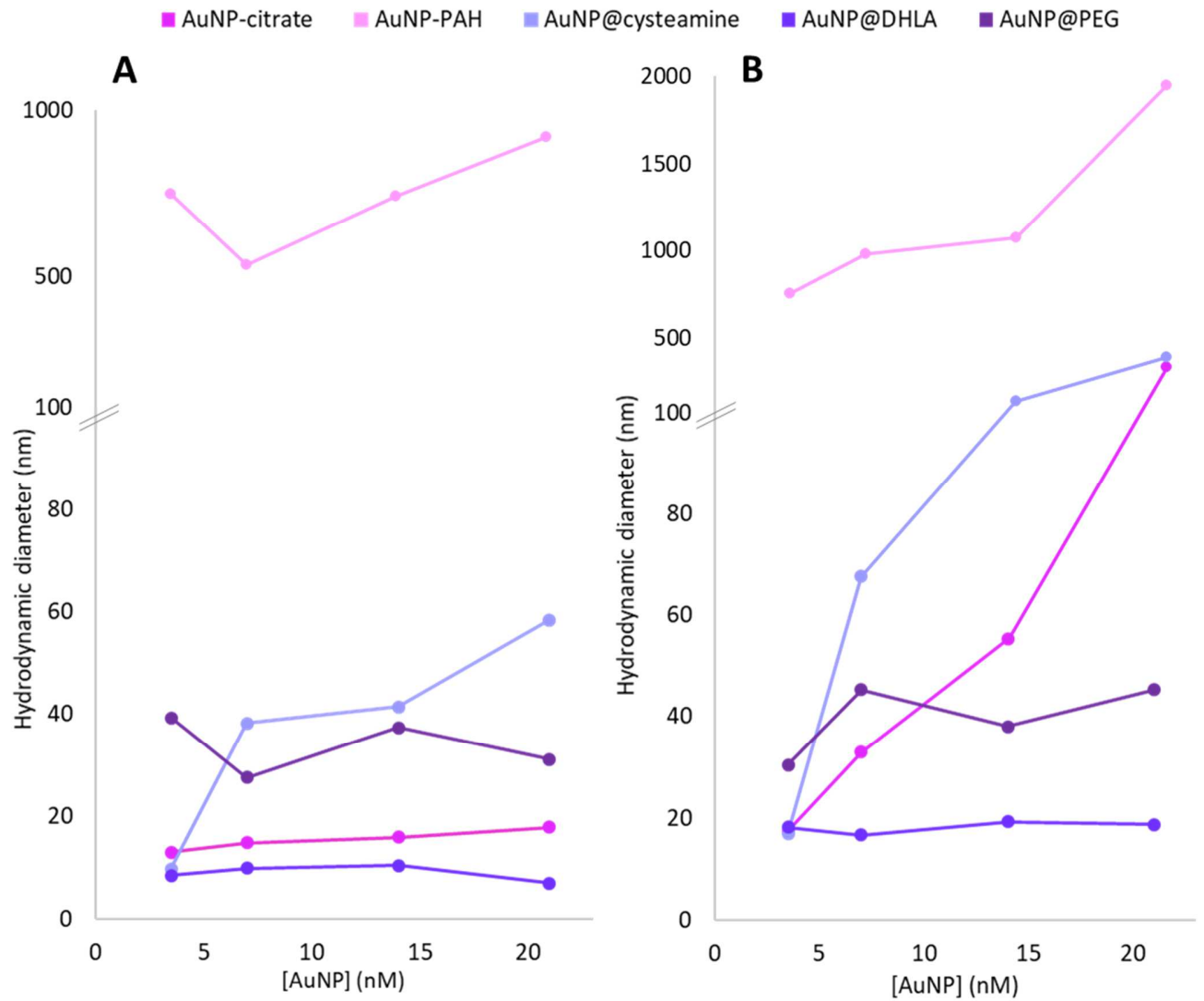


Figure 3. AuNP Dh measured by Dynamic Light Scattering. AuNP concentrations were increased from 3.5 nM to 21 nM in interaction with either albumin (A) or fibrinogen (B) which concentrations were fixed at 50 nM.

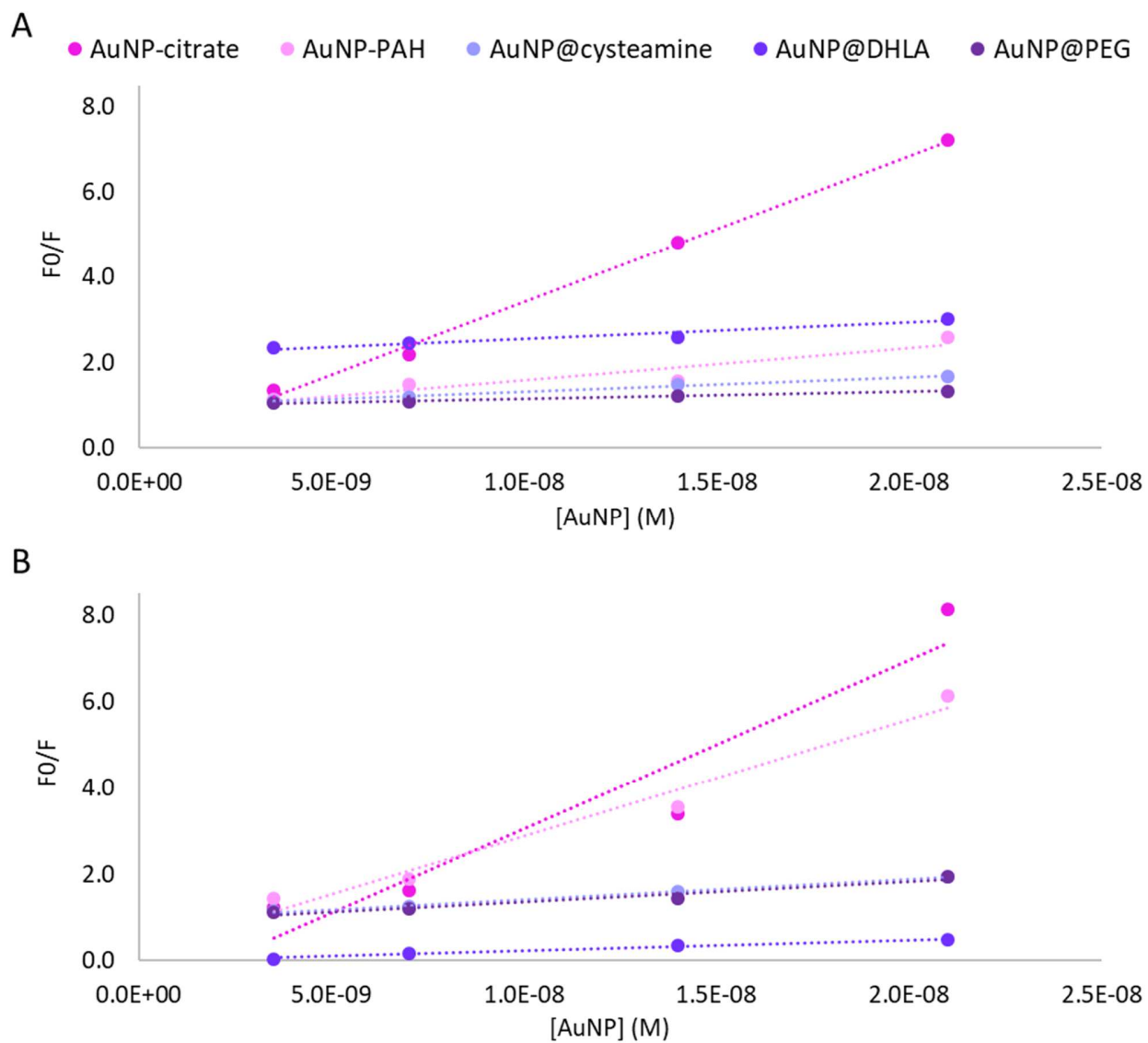


Figure 4. Stern-Volmer plot at 37 °C determined through fluorescence quenching of albumin (A) and fibrinogen (B) by an increasing concentration of AuNP.

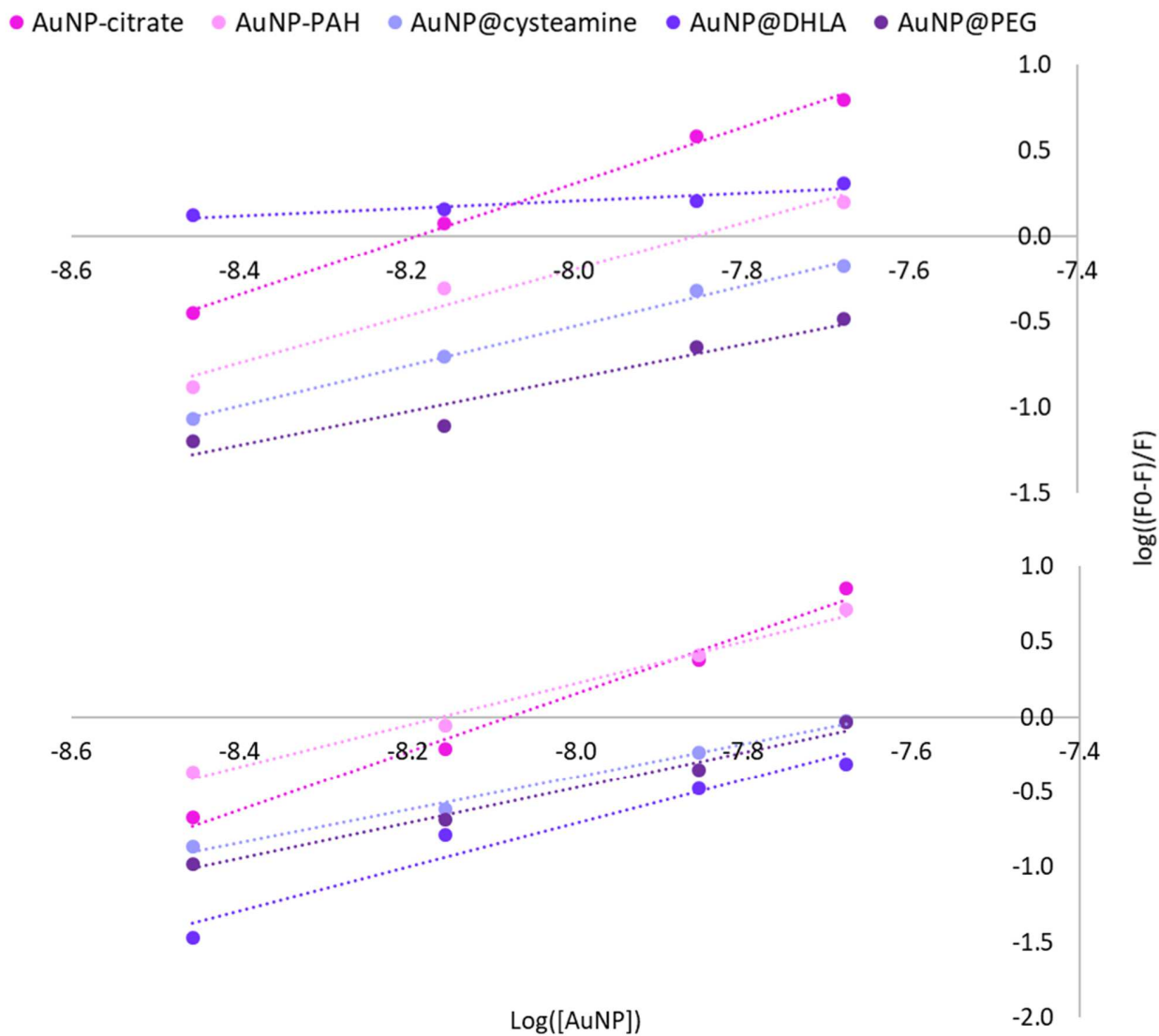


Figure 5. K_a plot at 37 °C determined through fluorescence quenching of albumin (A) and fibrinogen (B) by an increasing concentration of AuNP.

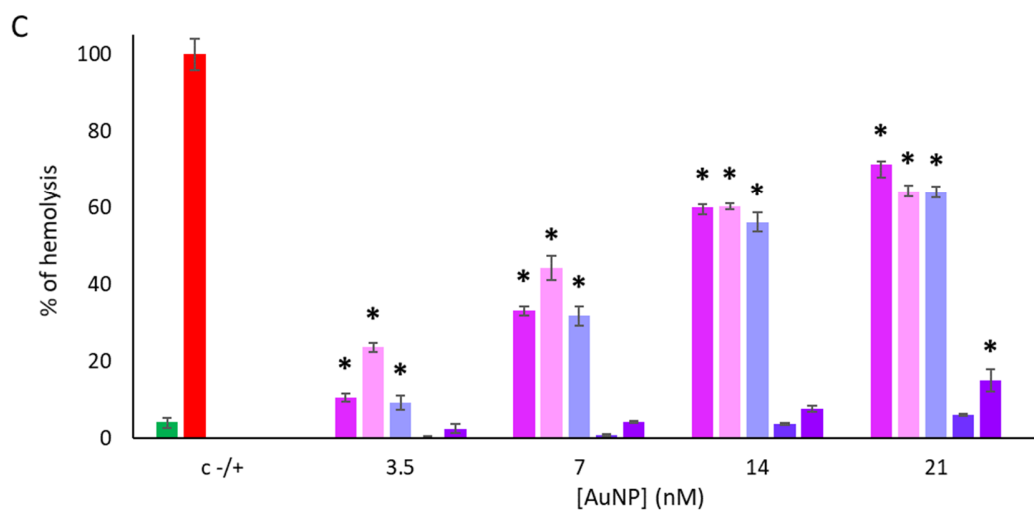
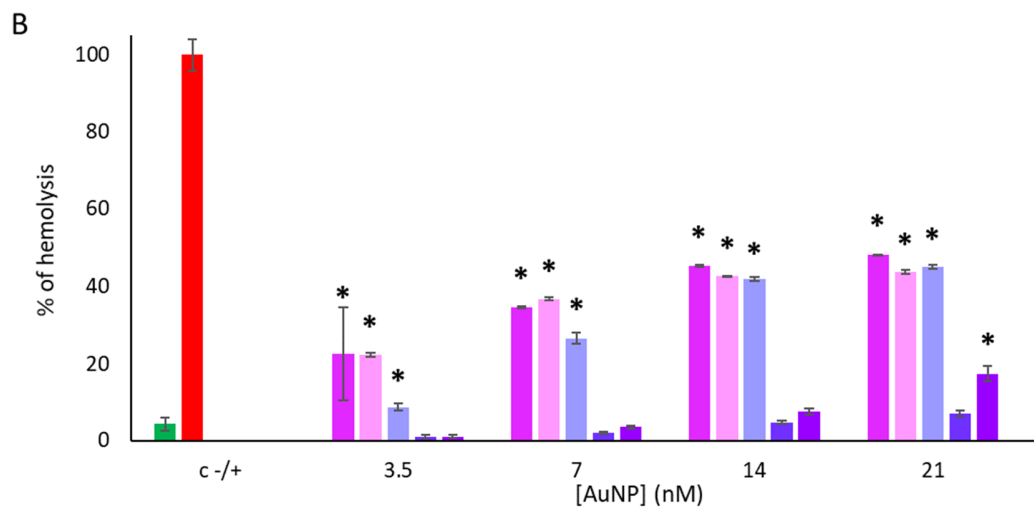
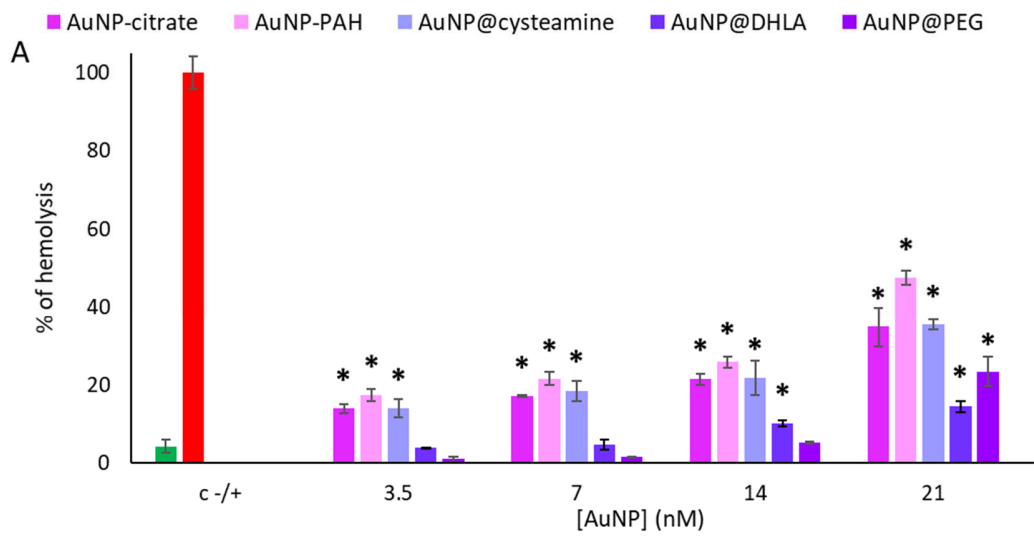


Figure 6. Hemolysis ratio (n = 3), errors bars represent the standard deviation) induced by an increasing concentration of AuNP in PBS (except for negative and positive controls) without proteins (A), or with either albumin at 50 nM (B) or fibrinogen at 50 nM (C). Statistical analyses were performed through two-way ANOVA followed by a post-hoc Bonferroni test (* p < 0.001 vs negative control)

Table 1. Physicochemical parameters of human proteins used in this study.

Physicochemical properties	Albumin	Fibrinogen
Molecular mass (g.mol ⁻¹)	69 000	340 000
Isoelectric point	4.7	5.8
Net charge at pH = 7.4 (mV)	-26	-38
Number of tryptophan residues accessible for quenching	1	25 ^a
Dimensions (nm)	7 × 6 × 4 ^b	9 × 47 × 6 ^c
Shape	Heart	Rodlike

a:(Gonçalves et al., 2007) b:(Erickson, 2009) c: (Cieśła et al., 2013)

Table 2: Physicochemical characterization of colloidal gold nanoparticles (n = 3 on three independent syntheses).

Physicochemical parameter	AuNP-Citrate	AuNP-PAH	AuNP@Cysteamine	AuNP@DHLA	AuNP@PEG
λ max (nm)	514 \pm 1	528 \pm 2	522 \pm 3	521 \pm 2	518 \pm 1
Hydrodynamic diameter Dh (nm)	5.8 \pm 0.9	11.9 \pm 0.7	10.5 \pm 1.5	8.4 \pm 0.9	28.5 \pm 0.5
Core diameter Dc (nm)	2.7 \pm 0.8	7.4 \pm 2.1	7.3 \pm 2.0	5.0 \pm 0.7	3.7 \pm 0.8
Zeta potential ζ (mV)	-32 \pm 1	31 \pm 3	28 \pm 2	-46 \pm 3	-4 \pm 2
Ligand binding Energy (kJ.mol ⁻¹)	11 ^a	25 ^b	188 ^c	188 ^c	188 ^c

a: energy per interaction Au-O involved in the stabilization of the gold core by citrate ions (Al-Johani et al., 2017), b: energy per interaction Au-N (Nuzzo et al., 1987) involved in the stabilization of the gold core by poly(allylamine), c: binding energy of a single thiol on AuNP gold core (Nuzzo et al., 1987), note that in the case of DHLA and PEG capping two thiols each ligand molecule is bound by two thiols.

Table 3. AuNP Dh and external layer thickness at a concentration of 7 nM.

AuNP concentration	Dh (nm)			External layer thickness (nm)	
	none	Albumin	Fibrinogen	Albumin	Fibrinogen
AuNP-citrate	5.8	14.8	32.9	12.1	Aggregation above 3.5 nM
AuNP-PAH	11.9	537	981	Aggregation	
AuNP@Cysteamine	4.4	38.2	67.7	Aggregation above 3.5 nM	
AuNP@DHLA	8.4	9.9	16.7	4.9	11.7
AuNP@PEG	28.3	27.5	45.3	23.8	41.6

Table 4. Albumin and fibrinogen fluorescence quenching constants at 37 °C. R stands for the correlation coefficient.

	Protein	AuNP ligand				
		Citrate	PAH	Cysteamine	DHLA	PEG
K_{sv} (L.mol ⁻¹)	Albumin	3.4×10^8	7.5×10^7	3.4×10^7	3.8×10^7	1.6×10^7
	Fibrinogen	3.9×10^8	2.7×10^8	4.7×10^7	2.6×10^7	5.0×10^7
K_q (L.mol ⁻¹ . s ⁻¹)	Albumin	3.4×10^{15}	7.5×10^{14}	3.4×10^{14}	3.8×10^{14}	1.6×10^{14}
	Fibrinogen	3.9×10^{15}	2.7×10^{15}	4.7×10^{14}	2.6×10^{14}	5.0×10^{14}
R	Albumin	0.9984	0.9343	0.9964	0.9708	0.9896
	Fibrinogen	0.9553	0.9861	0.9974	0.9932	0.9869

Table 5. Thermodynamics constants of AuNP- albumin or fibrinogen complexation at 37°C

	Protein	AuNP ligand				
		Citrate	PAH	cysteamine	DHLA	PEG
Hill coefficient	Albumin	1.6	1.2	1.2	0.2	1.0
	Fibrinogen	2.3	1.5	1.3	1.0	1.2
Ka	Albumin	1.8×10^{13}	4.8×10^{10}	6.3×10^8	8.1×10^1	3.1×10^7
	Fibrinogen	1.7×10^{18}	3.6×10^{12}	8.1×10^9	6.1×10^7	2.5×10^9
ΔS ($J.K^{-1}.mol^{-1}$)	Albumin	-432	-227	-501	-88	821
	Fibrinogen	574	-278	189	225	123
ΔH ($kJ.mol^{-1}$)	Albumin	-200	-106	-208	-37	207
	Fibrinogen	69	-157	104	-45	-18
ΔG ($kJ.mol^{-1}$)	Albumin	-65	-35	-53	-9	-48
	Fibrinogen	-54	-52	-48	-50	-56
Interaction	Albumin	H bound and Van Der Waals bound				Hydrophobic/ ionic
	Fibrinogen	Hydrophobic/ ionic	H bound and Van Der Waals bound	Hydrophobic/ ionic	Ionic	Ionic

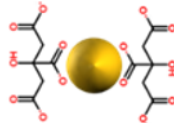
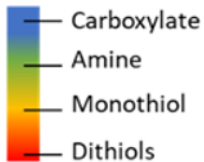
AuNP zeta potential

0

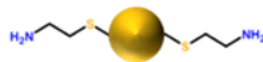


-50 50

Ligand binding energy



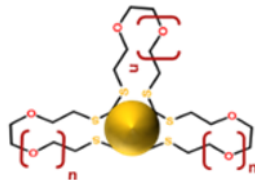
AuNP-Citrate



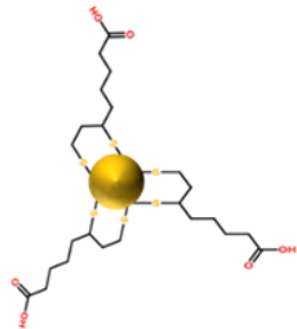
AuNP@Cysteamine



AuNP-PAH



AuNP@PEG



AuNP@DHHLA